Relationship between Hexamerization and ssDNA Binding Affinity in the uvsY Recombination Protein of Bacteriophage T4[†]

Richard A. Ando[‡] and Scott W. Morrical*

Department of Biochemistry, Department of Microbiology & Molecular Genetics, and Vermont Cancer Center, University of Vermont College of Medicine, Burlington, Vermont 05405

Received August 16, 1999; Revised Manuscript Received October 14, 1999

ABSTRACT: In bacteriophage T4, homologous genetic recombination events are catalyzed by a presynaptic filament containing stoichiometric quantities of the T4 uvsX recombinase bound cooperatively to single-stranded DNA (ssDNA). The formation of this filament requires the displacement of cooperatively bound gp32 (the T4 ssDNA-binding protein) from the ssDNA, a thermodynamically unfavorable reaction. This displacement is mediated by the T4 uvsY protein (15.8 kDa, 137 amino acids), which interacts with both uvsX− and gp32−ssDNA complexes and modulates their properties. Previously, we showed that uvsY exists as a hexamer under physiological conditions and that uvsY hexamers bind noncooperatively but with high affinity to ssDNA. We also showed that a fusion protein containing the N-terminal 101 amino acid residues of uvsY lacks interactions with uvsX and gp32 but retains both weak ssDNA-binding activity and a residual ability to stimulate uvsX-catalyzed recombination functions. Here, we present quantitative data on the oligomeric structure and ssDNA-binding properties of a closely related fusion protein designated uvsY*. Sedimentation velocity and equilibrium results establish that uvsY*, unlike native uvsY, behaves as a monomer in solution (M_{app} = 14.2 kDa, $s^0_{20,w}$ = 2.1). Like native uvsY, uvsY* binds noncooperatively to an etheno-DNA (ϵDNA) lattice with a binding site size of 4 nucleotides/monomer; however at physiological ionic strength, the association constant for uvsY*−ϵDNA is decreased 10^4-fold relative to native uvsY. Nevertheless, the magnitude of the salt effect on the association constant (K) is essentially unchanged between uvsY and uvsY*, indicating that disruption of the C-terminus does not disrupt the electrostatic ssDNA-binding determinants found within each protomer of uvsY. Instead, the large difference in ssDNA-binding affinities reflects the loss of hexamerization ability by uvsY*, suggesting that a form of intrahexamer synergism or cooperativity between binding sites within the uvsY hexamer leads to its high observed affinity for ssDNA.

Efficient replication of the genomic DNA of bacteriophage T4 is accomplished through the concerted reactions of both replication and recombination proteins. During T4 infection in *Escherichia coli*, a switch from the early, origin-dependent pathway of replication initiation to a highly prolific recombination-dependent mode of DNA synthesis occurs (*1*). This secondary initiation pathway requires the activities of T4 recombination proteins uvsX and uvsY, which generate the branched recombination intermediates that serve as primer-template junctions for replication (*2*−*5*). uvsX/uvsY-dependent homologous recombination is also important for phage survival of UV photodamage and DNA double-strand breaks (*6*−*8*). The uvsX and uvsY proteins are therefore of great interest in understanding the interdependent processes of DNA recombination, repair, and replication.

The uvsX protein is an ATP-dependent DNA strand transferase of the RecA family, catalyzing the homologous pairing, strand invasion, and branch migration phases of general recombination (*9*−*11*). The active form of uvsX protein is a presynaptic filament consisting of stoichiometric amounts of uvsX bound cooperatively to single-stranded DNA (ssDNA).[1] Quantitative analysis of uvsX−ssDNA interactions revealed a moderately strong cooperativity parameter of ω = 100, a binding site size of 4 nucleotide residues per monomer, and a relatively weak intrinsic affinity of uvsX for ssDNA at physiological ionic strengths (*12*).

The assembly and activities of uvsX−ssDNA presynaptic filaments are enhanced dramatically by the T4 uvsY protein (*5*, *13*, *14*). Genetics studies revealed that *uvsX*$^-$ and *uvsY*$^-$ mutants have identical recombination-deficient phenotypes (*15*−*18*). In vitro studies of uvsY effects on uvsX-catalyzed DNA strand exchange, ssDNA-dependent ATPase, and recombination-dependent DNA synthesis reactions demonstrated that uvsY enhances the interaction between uvsX and

[†] This work was supported by Research Grant GM48847 from the National Institutes of Health.

* To whom correspondence should be addressed: University of Vermont College of Medicine. Phone: (802) 656-8260. Fax: (802) 862-8229. E-mail: smorrica@zoo.uvm.edu.

[‡] Current address: Section of Microbiology, University of California−Davis, Davis, CA 95616.

[1] Abbreviations: ssDNA, single-stranded DNA; ϵDNA etheno-modified single-stranded DNA; SDS−PAGE, sodium dodecyl sulfate−polyacrylamide gel electrophoresis; KOAc, potassium acetate; gp32, bacteriophage T4 gene 32 protein; $uvsY_{NT}$, fusion protein containing uvsY amino acid residues 1−101 fused to a C-terminal hexahistidine affinity tag; ssb, ssDNA-binding protein; IPTG, isopropyl-β-D-thiogalactopyranoside; θ, fractional saturation of the DNA lattice with protein.

10.1021/bi991917h CCC: $18.00
Published on Web 11/23/1999

ssDNA, particularly in the presence of high concentrations of salt and of gp32, the T4-encoded ssDNA binding protein or ssb (*13*, *14*, *19*−*21*), i.e., conditions that approximate the physiological conditions encountered during T4 infection in *E. coli.* uvsX protein alone lacks sufficient affinity for ssDNA to efficiently displace tightly bound gp32 (*12*). However, uvsY mediates this displacement and thus promotes the formation of active presynaptic filaments (*22*, *23*). In mediating presynaptic filament assembly in the presence of a bound ssb protein, uvsY exhibits strong functional homologies with recombination mediator proteins in other systems, including the RecO/RecR proteins of *E. coli* and the Rad52 and Rad55/Rad57 proteins of *Saccharomyces cerevisiae* (*24*−*32*; reviewed in ref *33*).

The biochemical properties of uvsY protein point to a possible mechanism for its function in mediating presynaptic filament assembly. uvsY binds preferentially to ssDNA and exhibits specific protein−protein interactions with both uvsX and gp32 (*20*, *34*−*36*). The primary sequence of uvsY predicts a 137 amino acid polypeptide of 15.8 kDa mass; however, sedimentation studies revealed that uvsY exists predominantly as a hexamer (M_r = 95 kDa, $s^0_{20,w}$ = 6.0) in solution, and the hexameric structure is retained upon ssDNA binding (*37*). UV-cross-linking and sedimentation equilibrium results demonstrate that the ssDNA makes contact with multiple subunits of the same uvsY hexamer (H. T. H. Beernink and S. W. Morrical, manuscript in preparation). Binding to ssDNA results in a significant compaction of the uvsY hexamer (*37*). uvsY binds noncooperatively to an infinite ssDNA lattice, with a binding site size of 4 nucleotides/*monomer* and with an intrinsic affinity exceeding those of both gp32 and uvsX at physiological ionic strengths (*12*, *22*). Binding of uvsY to a fluorescent, etheno-derivatized ssDNA (ϵDNA) lattice leads in a salt-dependent manner to an unusually high degree of ϵDNA fluorescence enhancement (*22*). Finally, uvsY stoichiometrically cooccupies ssDNA molecules presaturated with gp32 and destabilizes the gp32−ssDNA complex in a manner independent of uvsY−gp32 protein−protein interactions (*38*). Together, the data suggest a model in which the interaction of uvsY hexamers with ssDNA alters the ssDNA structure in a way that disrupts the cooperative binding of gp32 to the lattice, allowing the recruitment of uvsX, displacement of gp32, and nucleation of presynaptic filaments (*22*, *33*, *37*, *38*).

Our model suggests that it is the hexameric structure of uvsY which plays a key role in altering ssDNA structure; therefore, it is desirable to test this model by procuring a form of uvsY that does not hexamerize. In this paper, we describe the biochemical properties of uvsY*, a fusion protein lacking the C-terminal 36 amino acid residues of native uvsY. Previous studies of a similar uvsY fusion protein (*20*) demonstrated that this truncated species (A) lacks protein−protein interactions with uvsX and gp32; (B) retains weak ssDNA-binding activity; and (C) retains the ability to weakly stimulate uvsX-catalyzed ssDNA-dependent ATPase and DNA strand exchange reactions. Here, we demonstrate using sedimentation velocity and equilibrium methods that uvsY* exists as a monomer in solution under a wide range of salt conditions, indicating that disruption of the C-terminus of uvsY abolishes hexamerization. We also present quantitative data on uvsY*−ssDNA interactions obtained via ϵDNA fluorescence enhancement assays. Our results indicate that disruption of uvsY's C-terminus abolishes hyperenhancement of ϵDNA fluorescence and greatly reduces its intrinsic affinity for ϵDNA. Nevertheless, other ssDNA-binding parameters are conserved between uvsY* and native uvsY, including the noncooperativity of binding, the binding site size, and the magnitude of the salt effect on the binding constant. Our results suggest that uvsY derives much of its binding energy for ssDNA from intrahexamer synergism or cooperativity between multiple binding sites within a hexamer.

MATERIALS & METHODS:

Reagents, Buffers, Enzymes, and Affinity Columns. All chemicals were of reagent grade; all aqueous buffers and solutions were made with filtered, deionized, glass-distilled water. All buffers and reagents used in fluorescence studies were sterile filtered at 0.45 μm. All chemicals and biochemicals were purchased from Sigma unless otherwise noted. ssDNA−cellulose affinity columns were prepared as described (*39*), using calf thymus DNA. All restriction enzymes were purchased from New England BioLabs, and all oligonucleotides were obtained from Operon Technologies. Native T4 uvsY protein was purified as described (*22*).

For the following buffer designations, the value of *x* equals the millimolar concentration of NaCl (or KOAc, as indicated). Chloride-based fluorescence buffers (CFB-*x*) contain 20 mM Tris-HCl, pH 7.5, and 1 mM $MgCl_2$, plus variable [NaCl]. Acetate-based fluorescence buffers (AFB-*x*) contain 20 mM Tris-OAc, pH 7.5, and 1 mM $Mg(OAc)_2$, plus variable [KOAc]. Analytical ultracentrifugation buffers (AnU-*x*) contain 20 mM Tris-HCl, pH 7.5, and 1 mM $MgCl_2$, plus variable [NaCl]. uvsY storage buffer (YSB) contains 20 mM Tris-HCl, pH 7.5, 1 mM $MgCl_2$, 0.2 mM EDTA, 1 mM 2-mercaptoethanol, 100 mM NaCl, and 60% (w/v) glycerol.

*Cloning, Expression, and Purification of uvsY**. The uvsY DNA sequences contained in uvsY* were PCR-amplified by standard procedures (*40*) from unmodified (C-containing) bacteriophage T4 genomic DNA (*41*) using the forward and reverse primers shown below:

Forward (25-mer):
5′-GCGGAATTCATGAGATTAGAAGATC-3′

Reverse (26-mer):
5′-CGGGATCCCTGCAACGAGGTATCAAC-3′

These primers introduce *Eco*RI and *Bam*HI restriction sites in the upstream and downstream sides, respectively, of the resultant PCR product. The amplified fragment was purified from unincorporated nucleotides and primers by centrifugation through Centri-Sep columns (Princeton Separations) following manufacturer's instructions and digested sequentially with *Bam*HI and *Eco*RI. The doubly digested insert and a similarly digested pTRcc99A vector (Pharmacia) were purified by LiCl precipitation following isolation from a low-melt agarose gel (*42*). The fragments were ligated to form plasmid pRAA1 and subsequently transformed into competent *E. coli* JM105 cells using standard procedures (*40*). Transformants were selected by growth on LB plates containing 50 μg/mL ampicillin. Individual clones were

screened for induction of uvsY* by adding 1 mM IPTG during log-phase growth in LB broth plus 50 μg/mL ampicillin and monitoring protein production by SDS−PAGE.

pRAA1 DNA from an overexpressing clone, selected as described above, was isolated and the sequence verified using a Dye-Deoxy DNA Sequencing Kit (Perkin-Elmer) and an ABI DNA sequencer. This construct encodes a predicted fusion protein (uvsY*) 121 residues in length and 13 915 Da in mass, in which the first 101 residues of uvsY are fused to three vector-encoded residues at the N-terminal end and 17 vector-encoded residues at the C-terminal end. The sequence of uvsY* is shown below, with uvsY-encoded sequences in boldface:

```
1   MEF MRLEDLQ EELKKDVFID STKLQYEAAN
31  NVMLYSKWLN KHSSIKKEML RIEAQKKVAL
61  KARLDYYSGR GDGDEFSMDR YEKSEMKTVL
91  SADKDVLKVD TSLQGSSRVD LQACKLGCFG
121 G
```

For large-scale induction of uvsY*, the JM105/pRAA1 cells were grown to $OD_{600} = 0.7$ in 6 L of LB plus 50 μg/mL ampicillin while shaking vigorously at 37 °C. Cells were induced with 1 mM IPTG and harvested by low-speed centrifugation 4 h postinduction. The pellet (typically 25 g wet weight/6 L of media) was quick-frozen in liquid N_2, and stored at −80 °C. Cell lysis and preparation of a cleared lysate by high-speed centrifugation was performed as described (*13*, *22*). Subsequent steps in the purification of uvsY* followed the same scheme as native uvsY (*22*), differing only in the chromatographic elution profiles, performed in the following sequence: uvsY* eluted from phosphocellulose at 500−550 mM NaCl in a 100 → 900 mM gradient, from ssDNA−cellulose in a 200 mM NaCl step, and from hydroxyapatite (HAP) at 600 mM potassium phosphate in a 100 → 900 mM gradient. During some uvsY* preparations a second ssDNA−cellulose chromatographic step was included as a final step to concentrate the final product. The final product was dialyzed into YSB and stored at −20 °C. uvsY* stock solutions were quantitated both by Bradford assay (using a wild-type uvsY stock as control) and by the absorbance at 280 nm using an extinction coefficient of $\epsilon_{M,280} = 12\,210\ M^{-1}\ cm^{-1}$ calculated from the amino acid sequence (*43*). All uvsY* stocks used in this study were judged >98% pure by SDS−PAGE and Coomassie Blue staining. uvsY* preps typically yielded 0.1 mg of purified protein/gram (wet weight) of induced cells. All uvsY* preps used in these studies were nuclease free according to previously described criteria (*22*).

Nucleic Acids. Circular single-stranded DNA from bacteriophage M13mp19 was isolated from purified phage particles as described (*44*, *45*). This ssDNA was used to make the fluorescent etheno-DNA (ϵDNA) derivative as described previously (*22*, *48*). The concentrations of both etheno-modified and -unmodified ssDNA species were determined by the phosphate-ash method (*47*, *48*). All ϵDNA and ssDNA concentrations are expressed in terms of nucleotide residues.

ϵDNA Fluorescence Enhancement Assays. Fluorescence experiments (forward stoichiometric, forward nonstoichiometric, salt-back, and competition titrations) were carried out in an SLM8000 fluorimeter essentially as described (*22*, *48*). Data in each titration were corrected for the effects of sample dilution, intrinsic protein fluorescence, inner filter effects, and/or baseline fluorescence of ϵDNA depending on the type of experiment (*22*, *48*, *49*). Protein-only titrations were performed to identify fluorescence change due to protein addition; this signal change was a linear function of protein concentration in all experiments. Data were not corrected for photobleaching of the ϵDNA, since photobleaching was found to be negligible over the time period of all experiments. Nevertheless, as a general precaution against photobleaching, samples were shielded from the light source at all times excepting the 10−15 s data acquisition interval following each addition and equilibration of titrant.

Salt-back-titration experiments (preformed uvsY*−ϵDNA complexes titrated with NaCl or KOAc) were carried out in CFB and AFB buffer systems as described (*22*, *48*). Starting concentrations of protein and ϵDNA are given in the figure legend. Forward titrations of ϵDNA with protein were carried out as described (*22*, *48*). Starting concentrations of ϵDNA are given in the figure legends. Buffer conditions included either CFB plus 10−70 mM NaCl or AFB plus 10−160 mM KOAc as indicated. Titrations at higher salt concentrations (nonstoichiometric binding conditions) were used to determine the affinity (K) and cooperativity (ω) parameters of uvsY*−ϵDNA interactions. Data were corrected, F_{max} values determined, and data reduced to terms of fractional saturation of the lattice (θ) as described previously for native uvsY protein (*22*). Data plotted as θ vs [uvsY*] were superimposed with theoretical binding isotherms generated from the equations of McGhee and von Hippel as described by Kowalczykowski et al. (*50*) for the noncooperative case. The goodness-of-fit of each theoretical isotherm to the data was estimated by inspection and adjusted if necessary by incrementally changing the F_{max} parameter for the data set (*12*, *22*, *46*).

Analytical Ultracentrifugation. Sedimentation velocity and equilibrium experiments were performed in a Beckman Optima XL-I analytical ultracentrifuge essentially as described (*37*). Sedimentation equilibrium studies were performed using the method of Yphantis (*51*). Initial loading concentrations of uvsY* ranged 0.8−1.5 mg/mL, and rotor speeds (An50-Ti rotor) ranged from 20 000 to 40 000 rpm. Concentration profiles were measured by the absorbance at 280 nm. Data editing and analyses of concentration profiles were performed as previously described (*37*, *52*−*54*), assuming molar mass (M) and partial specific volume ($\bar{\nu}$) values of 13 915 g/mol and 0.74 cm^3/g, respectively, for uvsY*, calculated from the amino acid sequence. SDS−PAGE was performed on samples before and after each equilibrium run and revealed no discernible degradation of the sample throughout the course of the experiment.

Sedimentation velocity data were analyzed using the $g(s^*)$ method of Stafford (*55*, *56*). Velocity runs were carried out in an An60-Ti rotor with cells containing 12 mm double-sector charcoal-filled Epon centerpieces and sapphire windows. Experiments were conducted at a rotor speed of 60 000 rpm and at protein concentrations of 0.8−1.5 mg/mL. Boundaries were measured by Rayleigh interference as described (*37*).

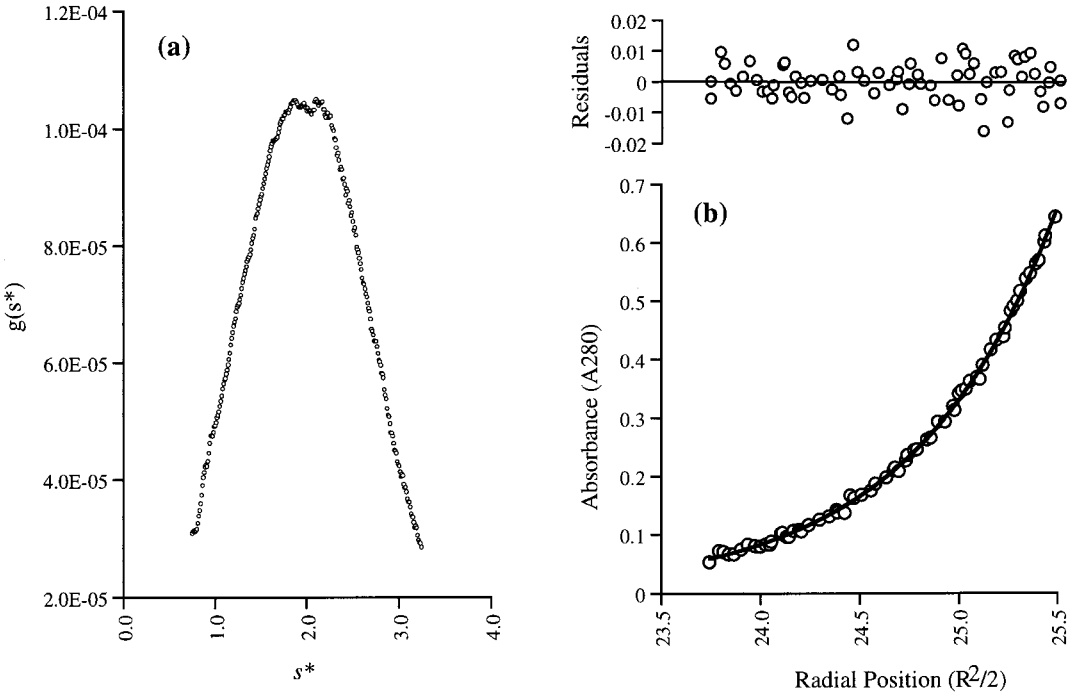

FIGURE 1: Sedimentation velocity and equilibrium studies of the uvsY* protein. (a) Sedimentation velocity of uvsY* protein in AnU-100 buffer at 22 °C. The time derivative of the concentration profile, $g(s^*)$, was obtained as described in Materials and Methods. Results of this and similar runs at different salt concentrations are summarized in Table 1. (b) Sedimentation equilibrium of uvsY* protein in AnU-500 buffer at 22 °C. Equilibrium runs were performed and data analyzed as described in Materials and Methods. Data were fit to an ideal, single component model. Results of this and similar runs at different salt concentrations are summarized in Table 1.

RESULTS:

uvsY vs uvsY$_{NT}$.* uvsY* contains the same uvsY sequences found in the previously described fusion protein uvsY$_{NT}$ (*20*) and differs from the latter only in the sequence of the C-terminal fusion peptide and in the presence of three additional residues at the N-terminus. uvsY$_{NT}$ was shown to (A) retain weak ssDNA-binding activity, (B) retain the ability to weakly stimulate uvsX-catalyzed ssDNA-dependent ATPase and DNA strand exchange reactions, and (C) lack protein−protein interactions with uvsX and gp32. Nevertheless, this histidine-tagged fusion protein exhibited poor solubility in solution and was unsuitable for quantitative studies of ssDNA-binding activity or aggregation state. The uvsY* species exhibits ssDNA-binding activity, stimulation of uvsX and lack of protein−protein interactions similar to uvsY$_{NT}$ but is significantly more soluble than uvsY$_{NT}$ (Y. Ma, W. Cooper, and S. W. Morrical, unpublished results). Hence, the uvsY* species is used for all of the solution studies reported here.

Sedimentation Velocity and Equilibrium Analyses of uvsY.* The native uvsY protein exists predominantly as a 6.0 S hexamer in AnU buffers containing NaCl concentrations greater than 200 mM, with larger oligomers of uvsY predominating below 200 mM NaCl (*37*). Sedimentation velocity and equilibrium methods were used to determine whether the uvsY* species is also capable of oligomerization. Sedimentation velocity results indicate that uvsY* comprises a single, monodisperse sedimenting species, with an estimated sedimentation coefficient of approximately 2.0 S at all salt concentrations tested (Figure 1a, Table 1). These results differ dramatically from those obtained previously with native uvsY protein. Conversely, the $s^0_{20,w}$ value for denatured, monomeric uvsY protein obtained in the presence of 6 M guanidinium-HCl was estimated to be <2.0 (*37*). Thus, our sedimentation velocity results suggest that, given the similar protomer masses of uvsY* and native uvsY (13.9 vs 15.8 kDa, respectively), uvsY* may behave as a monomer in solution under a wide range of salt conditions.

Table 1: Summary of Sedimentation Velocity and Equilibrium Results for uvsY*

(A) Sedimentation Velocity[a]	
[NaCl]	$s^0_{20,w}$
100 mM	2.143
500 mM	1.934
(B) Sedimentation Equilibrium[b]	
[NaCl]	M_r (Da)
100 mM	14 605 ± 866
300 mM	14 485 ± 1584
500 mM	13 628 ± 658
average	14 239 ± 1036

[a] Conditions for sedimentation velocity experiments are described in Materials and Methods. Sedimentation coefficients are corrected to zero concentration and 20 °C in water. Rayleigh interferometry was used in data collection. [b] Absorbance optics were used to collect sedimentation equilibrium data as described in Materials and Methods. For each salt concentration, global average molecular masses were determined from runs at three different protein concentrations. The net average from experiments at all three salt concentrations is indicated on the bottom line.

The monomeric state of uvsY* was confirmed by sedimentation equilibrium. Scans obtained at multiple loading concentrations and rotor speeds were globally fit to an ideal single-component model. A representative scan is shown with best-fit exponential in Figure 1b, which yielded an apparent mass of 14.6 ± 0.9 kDa for uvsY*. Similar values were obtained at higher salt concentrations (Table 1), for an

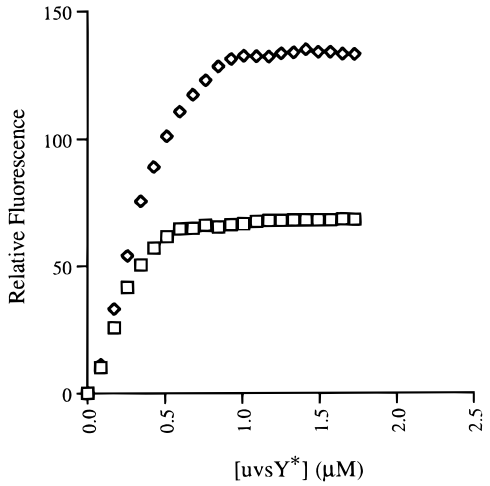

FIGURE 2: Forward titrations of ϵDNA with uvsY* protein under stoichiometric (low-salt) binding conditions. Titrations were carried out at 25 °C in a quartz cuvette containing a 2.0 mL starting volume of CFB-10 buffer with either 2.1 μM (□) or 4.2 μM (◊) ϵDNA. The increase in ϵDNA fluorescence due to binding of uvsY* was monitored at 405 nm while exciting at 300 nm as described (*22*). Data were corrected for intrinsic protein fluorescence, for the fluorescence of free ϵDNA, and for dilution and inner filter effects. See Materials and Methods.

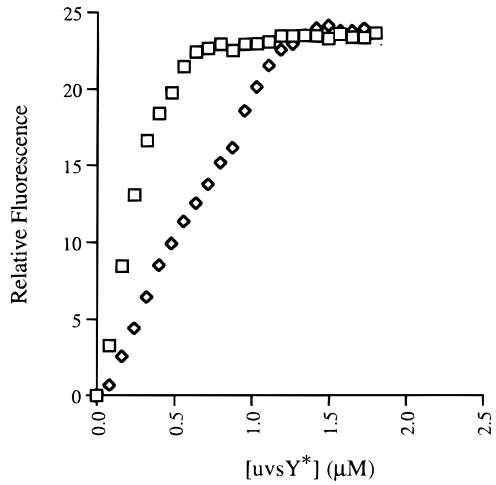

FIGURE 3: Competition titration of ϵDNA and unmodified ssM13mp19 lattices with uvsY* protein. An estimate of the relative affinities of uvsY* for etheno-modified vs native M13mp19 ssDNA was made by comparing forward titrations of uvsY* onto 2.1 μM ϵDNA alone (□) or 2.1 μM ϵDNA plus 2.1 μM unmodified M13mp19 ssDNA (◊), both in CFB-10 buffer. See text.

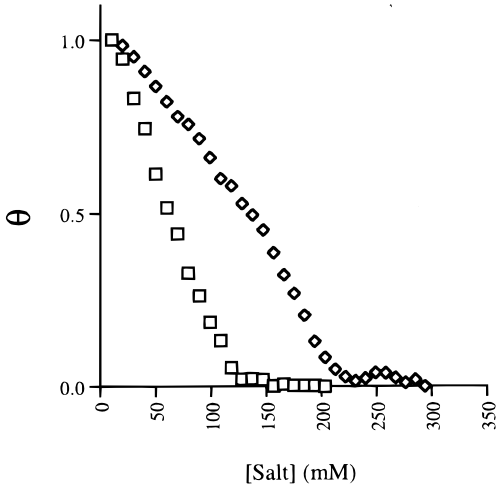

FIGURE 4: Salt-back-titrations of preformed uvsY*−ϵDNA complexes. The salt-dependent dissociation of a saturated 1:1 complex of uvsY* (0.52 μM) and ϵDNA (2.1 μM) is shown upon titration of the preformed complex with either concentrated NaCl (□) or KOAc (◊) as described in Materials and Methods. Data were corrected for dilution and for protein fluorescence. The parameter θ represents fractional saturation of the ϵDNA lattice with protein. The initial relative fluorescence signal was assigned a value of $\theta = 1$, and the baseline signal following complete dissociation was assigned a value of $\theta = 0$. All intermediate points were normalized against the upper limit of $\theta = 1$.

overall, salt-independent average of $M_{app} = 14.2 \pm 1.0$ kDa. The calculated mass of uvsY* (from amino acid sequence) is approximately 13.9 kDa. Therefore, we conclude that this altered and truncated form of uvsY protein is unable to self-associate and exists as a monomer under all salt conditions tested. The equilibrium sedimentation behavior of uvsY* differs dramatically from that of native uvsY, which exists exclusively as a 95 kDa hexamer at NaCl concentrations of >300 mM and as equilibria of hexamers and higher-order oligomers at NaCl concentrations < 300 mM (*37*).

Stoichiometry of uvsY−ssDNA Interactions.* The binding site size of uvsY* on a single-stranded DNA lattice was measured by means of the ϵDNA fluorescence enhancement assay. This assay was previously employed in quantitative studies of native uvsY-ssDNA interactions (*22*). Results are shown in Figure 2. Forward titrations of ϵDNA with uvsY* were performed under low-salt, stoichiometric binding conditions in both chloride (CFB-10) and acetate (AFB-10) buffer systems. These salt conditions allowed the strongest binding seen in salt-back-titrations performed to examine uvsY*−ϵDNA salt stability (see Figure 4). Figure 2 shows titrations of two different concentrations of ϵDNA with uvsY* at 10 mM NaCl. At both lattice concentrations, fluorescence increases approximately linearly with uvsY* concentration until a plateau is reached representing the saturation of lattice with protein. The intersection of lines (not shown) drawn through the linear ascending and plateau regions gives the apparent break point of the titration curve, which at both lattice concentrations yielded a binding site size of $n = 4$ nucleotide residues per uvsY* monomer. Identical results were obtained in 10 mM KOAc (data not shown), indicating that the NaCl and KOAc salts do not differentially affect the binding site size of uvsY* on ϵDNA. Separate preparations of both uvsY* and the ϵDNA lattice were tested with identical results. The binding site size of uvsY* is identical to that of native uvsY (*22*).

An important difference between uvsY* and native uvsY was noted in the raw data for Figure 2 (not shown). uvsY* produces a 2.2-fold enhancement of ϵDNA fluorescence at saturation in these titrations performed at low salt, a degree of enhancement similar to several other protein species (*46*, *57*, *58*). Data presented in later sections (see Figures 4 and 5) indicates that the degree of uvsY* fluorescence enhancement is independent of salt concentration. In contrast, native uvsY produces a markedly larger enhancement of ϵDNA fluorescence at low salt (3.5−6-fold), but the degree of enhancement decreases with increasing salt concentration (*22*). The molecular nature of native uvsY's hyperenhancement of ϵDNA fluorescence is currently unknown.

uvsY Has Approximately Equal Affinities for Etheno-modified vs Unmodified ssDNA.* Studies employing ϵDNA as a model lattice established that the affinity preference for

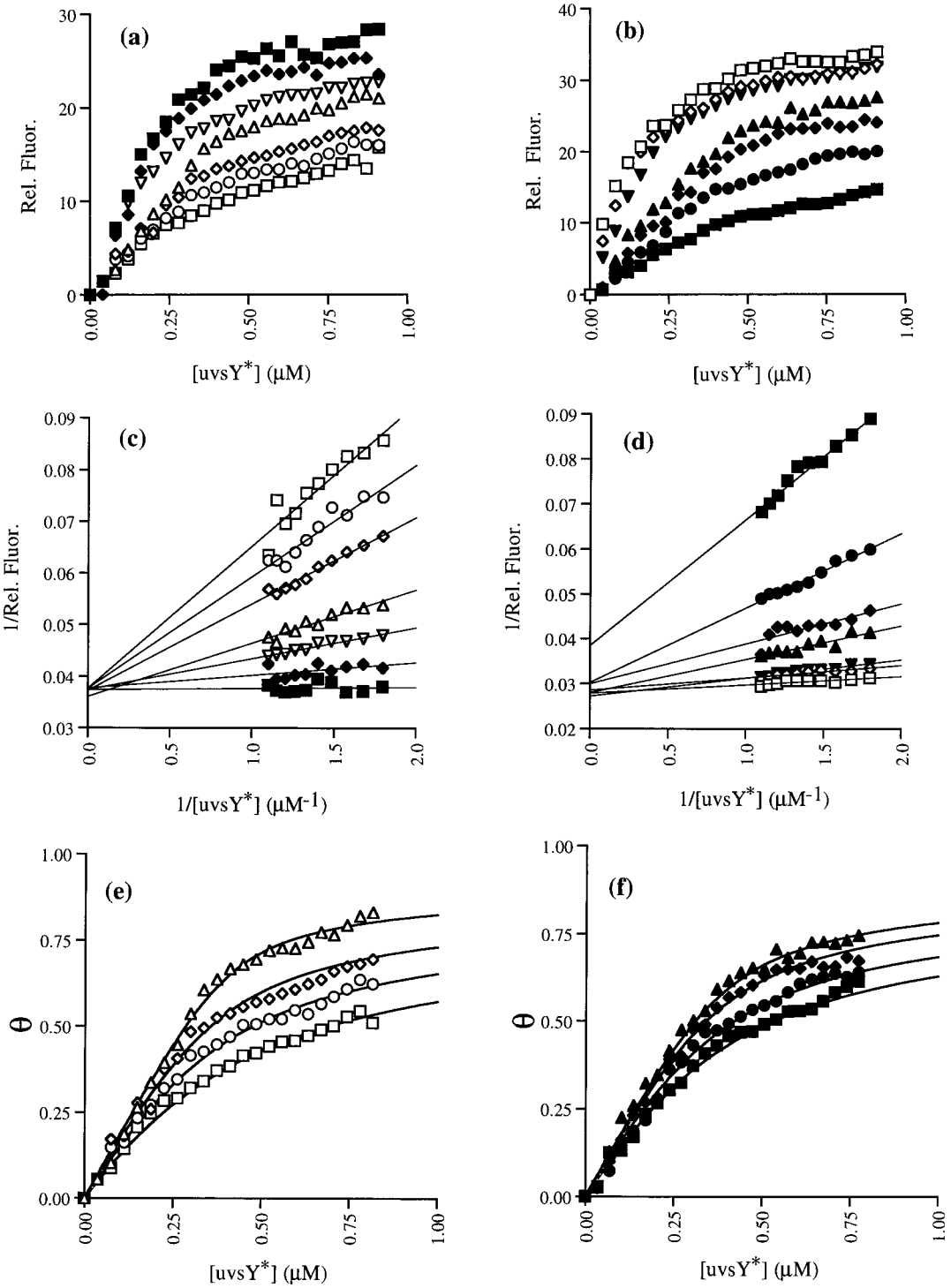

FIGURE 5: Forward titrations of ϵDNA with uvsY* at increasing salt concentrations; estimation of affinity constant (*K*) and cooperativity (*ω*) parameters from nonstoichiometric binding isotherms. Titrations were performed in CFB (panels a, c, and e) and AFB (panels b, d, and f) buffer systems with NaCl and KOAc concentrations as indicated below. For experiments with NaCl, concentrations were as follows: 10 mM (■), 20 mM (♦), 30 mM (▽), 40 mM (△), 50 mM (◊), 60 mM (○), 70 mM (□) NaCl. For experiments with KOAc, concentrations were as follows: 50 mM (□), 100 mM (◊), 120 mM (▼), 130 mM (▲), 140 mM (♦), 150 mM (●) and 160 mM (■) KOAc. Data symbols are consistent between NaCl experiments (panels a, c, and e) and between KOAc experiments (panels b, d, and f). Panels a and b show titrations as relative fluorescence values corrected for the fluorescence of protein and free ϵDNA, dilution, and inner filter effects. Panels c and d show double reciprocal plots derived from the final 10 data points of each titration shown in panels a and b, which were used to estimate maximum fluorescence signals (F_{max} values) for each titration as described in the text. Panels e and f show titration data expressed as fractional saturation of the ϵDNA lattice with protein (*θ*), with best-fit theoretical binding isotherms overlaid for each of four selected titrations. The theoretical isotherms were generated by the McGhee−von Hippel equation for noncooperatively binding proteins as described (*50*, *59*, *62*). Affinity (*K*) parameters derived from these isotherms are listed in Table 2.

the etheno-modified vs unmodified ssDNA may vary significantly between protein species (*12*, *22*, *46*, *48*, *57*, *58*). Wild-type uvsY protein shows an approximately 2−6-fold higher affinity for ϵDNA than for unmodified ssDNA (*22*). Is the same true for uvsY*? Figure 3 shows a competition titration (open diamonds) in which an equimolar mixture of

unmodified M13mp19 ssDNA and M13mp19-derived ϵDNA is titrated with uvsY*. A similar titration containing the ϵDNA lattice alone is shown in Figure 3 (open squares) for direct comparison. In both cases, we are specifically detecting uvsY*−ϵDNA binding by monitoring the increase in ϵDNA fluorescence. In the presence of equimolar unmodified ssDNA, the ascending portion of the titration curve remains approximately linear, but its slope is decreased 2-fold with regard to the titration with ϵDNA alone (Figure 3). Likewise, the apparent endpoint of the titration is increased by a factor of 2 when equimolar unmodified ssDNA is present (Figure 3). If uvsY* had a strong preference for ϵDNA, then the addition of unmodified ssDNA would have little or no effect on the titration curve. Alternatively, if uvsY* had a strong preference for unmodified ssDNA, then its addition would cause a lag or sigmoidicity to appear in the titration curve. Neither of these being the case, the results in Figure 3 indicate that uvsY* has very similar affinities for unmodified vs etheno-modified DNA and probably binds distributively between the two lattices. Thus, uvsY* varies significantly in this regard from native uvsY, which shows a moderate preference for ϵDNA (*22*).

Salt Stability of the uvsY−ϵDNA Complex.* Salt-back-titrations of the uvsY*−ϵDNA complex with NaCl and KOAc are shown in Figure 4. Titrations of this nature are used to determine the ranges of salt concentrations that allow stoichiometric vs nonstoichiometric binding, as well as to identify specific ion effects on binding. The data indicate that the uvsY*−ϵDNA complex is very sensitive to disruption by salt. In fact, stepwise dissociation of uvsY*−ϵDNA is observed with each salt addition beginning at either 10 mM NaCl or KOAc, the lowest salt concentrations tested, resulting in the complete absence of a plateau or range of stability at low salt concentrations (Figure 4). Nevertheless, the relatively sharp titration endpoints seen in Figure 2 indicate that binding of uvsY* to ϵDNA is stoichiometric or nearly so at 10 mM salt. The dissociation midpoints for the uvsY*−ϵDNA complex occur at NaCl and KOAc concentrations of 65 and 145 mM, respectively, values much lower than the corresponding midpoints for the native uvsY−ϵDNA complex [440 and 720 mM, respectively (*22*)]. The uvsY*−ϵDNA complex appears to be completely dissociated at concentrations of 120 mM NaCl and 220 mM KOAc, respectively (Figure 4). Note that the uvsY*−ϵDNA complex is significantly more stable in the presence of acetate counterion than in the presence of chloride. This result is consistent with anion displacement during complex formation and parallels results obtained with native uvsY (*22*). The anion displacement phenomenon is explored further in a later section. Note also that titrations with KCl produced identical results to the NaCl titrations (data not shown), indicating the absence of a specific monovalent cation effect on the stability of the uvsY*−ϵDNA complex.

Evaluation of Affinity (K) and Cooperativity (ω) Parameters for uvsY−ϵDNA Interactions.* To determine the values of the affinity and cooperativity parameters for uvsY*−ϵDNA binding required the analysis of binding isotherms generated under nonstoichiometric binding conditions, i.e., at intermediate salt concentrations yielding partial dissociation of uvsY*−ϵDNA as measured in Figure 4. Figure 5a shows corrected fluorescence data for a series of titrations performed in CFB buffer containing 10−70 mM NaCl. Figure 5b shows a similar series of titrations performed in AFB buffer containing 50−160 mM KOAc. The chosen NaCl and KOAc concentrations bracket the midpoints of the salt-back-titrations shown in Figure 4. Qualitative analysis of the titration data in Figure 5, panels a and b, reveals some important features: (A) the titration curves are completely lacking in sigmoidicity, suggesting the absence of cooperativity (i.e., $\omega = 1$) in uvsY*−ϵDNA binding under all salt conditions examined; (B) binding to the ϵDNA lattice appears nonstoichiometric at salt concentrations above 30 mM NaCl and 120 mM KOAc, respectively; (C) the maximum fluorescence signal (F_{max}) of each titration appears to converge upon a common value; and (D) salt ranges where nonstoichiometric binding is best observed appear to fall around the midpoints of salt-back-titrations (Figure 4), as expected.

Assuming values of $n = 4$ and $\omega = 1$, respectively, for the binding site size and cooperativity parameters of uvsY* allows us to determine the value of K at each salt concentration by fitting theoretical, noncooperative binding isotherms generated from the equations of McGhee and von Hippel (*59*) to the experimental data. To do so requires accurate knowledge of the titration half-saturation point, $L_{T,0.5}$, which in turn requires an accurate estimate of the maximum fluorescence signal, F_{max}. To obtain good estimates for F_{max}, we plotted the final 10 points of each titration in double-reciprocal form, as shown in Figure 5, panels c and d. A least-squares line fitted to the data in this form gives, for each data set, a value of F_{max} equal to the reciprocal of the vertical intercept. A similar approach was used to estimate F_{max} values for native uvsY (*22*). Treatment of the NaCl data sets in this fashion resulted in lines that appeared to intercept the vertical axis at a common point (Figure 5c), indicating a common F_{max} value for titrations in 10−70 mM NaCl. An F_{max} value representing the average value for all titrations was used in all subsequent calculations with the NaCl data sets. Similar behavior was noted for the KOAc data sets (Figure 5d); only the data at the highest KOAc concentration (160 mM) yielded an F_{max} value significantly lower than those obtained at other KOAc concentrations. Thus, for all KOAc concentrations except 160 mM, the average F_{max} value was used in subsequent calculations, while the 160 mM KOAc data was processed using its own independent F_{max} value.

By normalizing against the F_{max} values obtained from Figure 5, panels c and d, the data were converted into terms of fractional saturation of the lattice, θ. At the four highest NaCl and KOAc concentrations shown in Figure 5, panels a and b (where nonstoichiometric binding occurs), the half-saturation point, $L_{T,0.5}$, was determined from the uvsY* concentration at which the data appeared to cross the $\theta = 0.5$ threshold. Values of $L_{T,0.5}$ were used to calculate K, and these corresponding K values were used to generate theoretical isotherms at each salt concentration of ≥40 mM NaCl or 130 mM KOAc as described (*50*), assuming n and ω parameter values of 4 and 1, respectively. The K-values obtained are listed in Table 2, and the theoretical isotherms generated are shown in comparison to experimental data in Figure 5, panels e and f. Visual inspection showed that the theoretical isotherms appeared to fit the experimental data quite reasonably. Clearly, uvsY* binds noncooperatively to ϵDNA as indicated by the ability of this theoretical model to adequately represent the experimental data in all cases.

Table 2: Values of the Intrinsic Affinity Constant (K) for uvsY*−ϵDNA Interactions as a Function of Salt Concentration

salt	concentrated (mM)	K (M^{-1})[a]	$K_{Mg-corr}$ (M^{-1})[b]
NaCl	40	2.17×10^7	9.22×10^7
NaCl	50	5.28×10^6	1.61×10^7
NaCl	60	2.30×10^6	5.55×10^6
NaCl	70	1.14×10^6	2.34×10^6
KOAc	130	1.03×10^7	1.37×10^7
KOAc	140	6.30×10^6	8.12×10^6
KOAc	150	3.10×10^6	3.89×10^6
KOAc	160	1.83×10^6	2.24×10^6

[a] uvsY*−ϵDNA association constants calculated from the best-fit theoretical curve overlaid upon experimental data (Figure 5, panels e and f) using the McGhee−von Hippel equation (*50*, *59*, *62*) for a noncooperatively binding ligand on an infinite lattice, as described in Materials and Methods. [b] Association constants corrected for Mg^{2+} effects as described (*60*).

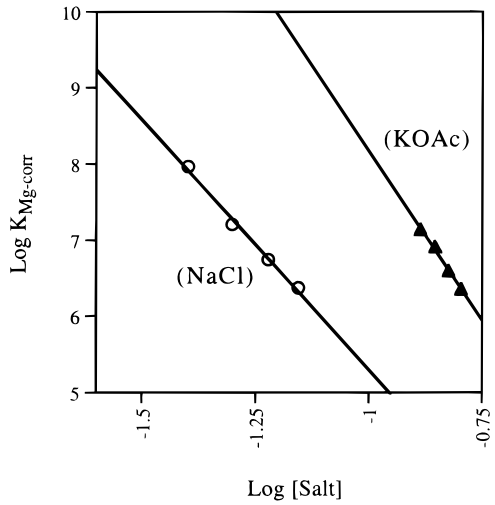

FIGURE 6: Salt effects on the affinity ($K_{Mg-corr}$) parameter for uvsY*−ϵDNA interactions. Mg^{2+}-corrected intrinsic affinity data (Table 2) are plotted in log−log format vs NaCl (○) or KOAc (▲) concentration. The magnitudes of the individual salt effects on $K_{Mg-corr}$ are determined from the slopes of these plots (e.g., d log $K_{Mg-corr}$/d log[salt]), which had values of −6.5 and −8.9 for the NaCl and KOAc data, respectively.

The noncooperative binding behavior of uvsY* parallels that of native uvsY (*22*). Of further interest is the relatively large salt effect on the K parameter (Table 2), which we explore quantitatively in the following section.

Salt Effects on the K Parameter. The number of monovalent ions displaced during protein−nucleic acid binding may be estimated from the slope of a log−log plot of $K_{Mg-corr}$, the K parameter corrected for the effects of Mg^{2+} ions, vs [salt] according to the formula

$$\text{d log } K_{Mg-corr}/\text{d log[salt]} = -m'\psi - a \qquad (1)$$

where m' equals the number of ionic contacts formed between the protein and DNA phosphate residues, ψ equals the fraction of ions thermodynamically bound to the DNA (a value of 0.71 for ssDNA), and a equals the number of anions displaced through binding (*60*).

The K values obtained for uvsY* were corrected for Mg^{2+} effects as described (*60*); the corrected values are listed in Table 2 and plotted in Figure 6. Linear least-squares fits of the data yielded slopes of −6.5 and −8.9 for the NaCl and KOAc data, respectively (Figure 6). If we assume a maximum value of 4 for the m' parameter, given a binding site size of $n = 4$, then the a parameter has a minimum value of 3.66 (from the slope of the NaCl data), indicating that at least three to four anions are displaced from each uvsY* monomer upon binding to the single-stranded lattice. The displacement of anions during uvsY*−ϵDNA binding accounts for the large enhancement in the relative stability of the complex in the presence of acetate vs chloride ions, as predicted by the Hoffmeister series (*61*).

Extrapolation of the NaCl data in Figure 6 to a concentration of 200 mM (approximating physiological ionic strength) yields an estimated K value of 2.3×10^3 M^{-1} for uvsY*−ssDNA interactions, which is roughly 4 orders of magnitude lower than the estimate of $\sim 1 \times 10^7$ M^{-1} for native uvsY (*22*). However, the slope obtained from the uvsY*/NaCl data (−6.5; Figure 6) is nearly identical to that obtained for native uvsY [−6.8 (*22*)], whereas the slope obtained from the uvsY*/KOAc data (−8.9; Figure 6) is greater than that obtained for native uvsY [−6.1 (*22*)]. It is not clear whether the latter represents a real difference between uvsY* and native uvsY or merely an artifact due to the much smaller range of KOAc concentrations used in this study. Nevertheless, the similarity in d log $K_{Mg-corr}$/d log[NaCl] values between the two uvsY species is significant since it indicates that the ionic component of polynucleotide binding is unchanged upon removal of the C-terminal 36 amino acid residues of uvsY. This comparison suggests that it is the loss of hexamer-forming ability by uvsY*, not loss of ssDNA-binding site determinants within the uvsY* monomer, that accounts for the large difference in ssDNA-binding affinities between the two uvsY species. This possibility is explored further below.

DISCUSSION

The 101 N-terminal amino acid residues of the bacteriophage T4 uvsY protein were cloned and expressed in an IPTG inducible fusion protein, uvsY*. The biophysical properties of uvsY* exhibit dramatic differences from, as well as some striking similarities to, the properties of native uvsY protein, which we outline below:

The modifications of the native uvsY sequence found in uvsY*, which include a 36 residue truncation of the C-terminus, disrupt the hexameric quaternary structure of uvsY as demonstrated by changes in sedimentation properties [Figure 1, Table 1 (*37*)]. These results suggest that sequence determinants required for uvsY hexamerization may reside within the previously defined C-terminal domain of this protein (*20*), although this cannot be stated with certainty due to the presence of fusion sequences at the N- and C-termini of uvsY*, which could conceivably interfere with hexamerization in other ways. The modifications present in uvsY* also severely attenuate the ssDNA-binding affinity of this species compared to native uvsY, and cause other changes in polynucleotide-binding properties [Table 2, Figures 2−5 (*22*)]. Nevertheless, key parameters of the uvsY−ssDNA interaction are conserved within uvsY*, including the binding site size, the noncooperativity of binding, and the magnitude of the salt effect on the binding constant [Figures 2, 5, and 6 (*22*)]. Conservation of these key parameters indicates that truncation of the C-terminus of uvsY does not disrupt the electrostatic ssDNA-binding

determinants found within each uvsY protomer. Therefore, a more likely explanation for the decrease in ssDNA-binding affinity observed in uvsY* vs uvsY is the loss of hexamer-forming ability in the former, indicating that synergism or cooperativity of binding between multiple protomers within a uvsY hexamer leads to the large intrinsic ssDNA-binding affinity observed with the native protein (*22*).

Yassa et al. (*20*) demonstrated that partial chymotrypsinolysis of uvsY protein yields as its major product an 11.5 kDa fragment consistent with the N-terminal 101 amino acid residues of uvsY. Expression of these residues coupled to a C-terminal histidine affinity tag produced the species designated $uvsY_{NT}$, a protein identical to uvsY* save for a different C-terminal fusion sequence and an unmodified N-terminus. Both fusion proteins exhibit a qualitatively similar ssDNA-binding activity and a similar lack of protein−protein interactions with T4 recombination proteins uvsX and gp32 (ref *20*; Y. Ma, W. Cooper, and S. W. Morrical, unpublished results). The results of the current study, demonstrating conservation of electrostatic ssDNA-binding determinants between uvsY* and native uvsY, support our earlier conclusion (*20*) that the N-terminal 101 residues of uvsY contain the ssDNA-binding site and constitute the ssDNA-binding domain of the protein. While the work of Yassa et al. (*20*) suggested that sequence determinants residing in the C-terminal 36 residues of uvsY are essential for protein−protein interactions with uvsX and gp32, the current study raises another interesting possibility—that the latter two proteins only interact with the hexameric form of uvsY. This issue may only be resolvable through further work on the structure of uvsY protein and the stoichiometries of its heteroassociations.

The current model for uvsY-dependent assembly of the T4 presynaptic filament (*33*, *37*, *38*) holds that uvsY hexamers interact with and destabilize gp32−ssDNA complexes by wrapping or kinking the ssDNA in such a way that the high cooperativity of gp32−ssDNA interactions is reduced. This creates "weak spots" in the gp32−ssDNA complex wherein the uvsX recombinase may be recruited to the ssDNA, nucleating uvsX−ssDNA filament formation while displacing gp32. This model is supported by a number of observations including (A) that uvsY hexamers bind to ssDNA as intact units with multiple subunits contacting the ssDNA (ref *37*; H. T. H. Beernink and S. W. Morrical, manuscript in preparation); (B) that uvsY binds stoichiometrically to gp32−ssDNA complexes without displacing gp32 from the ssDNA directly (*38*); and (C) that uvsY destabilizes gp32−ssDNA complexes in a manner independent of uvsY−gp32 protein−protein interactions (*38*). The model predicts that the hexameric structure of uvsY is critical for creating the distortions in ssDNA structure that destabilize gp32−ssDNA interactions and that conceivably form optimal assembly sites for the uvsX recombinase. Seen in this light, the inability to form hexamers may be the most important molecular defect of uvsY species with disrupted C-termini such as uvsY* and $uvsY_{NT}$, overshadowing their loss of heteroprotein associations, and may explain the dramatically weakened abilities of these species to stimulate uvsX-catalyzed DNA strand exchange and ssDNA-dependent ATPase reactions in vitro (ref *20*, and unpublished results).

ACKNOWLEDGMENT

The authors wish to thank Dr. Hans Beernink of this laboratory for his assistance with analytical ultracentrifugation experiments and Dr. Mark Sweezy of this laboratory for discussion and feedback. We also thank David Yassa, Yujie Ma, and Wendy Cooper of this laboratory for their technical assistance.

REFERENCES

1. Kreuzer, K. N., and Morrical, S. W. (1994) in *Molecular Biology of Bacteriophage T4* (Karam, J. D., Ed.) pp 28−42, American Society for Microbiology, Washington DC.
2. Kreuzer, K. N., Yap, W. Y., Menkens, A. E., and Engman, H. W. (1988) *J. Biol. Chem. 263*, 11366−73.
3. Luder, A., and Mosig, G. (1982) *Proc. Natl. Acad. Sci. U.S.A. 79*, 1101−5.
4. Mosig, G. (1987) *Annu. Rev. Genet. 21*, 347−71.
5. Formosa, T., and Alberts, B. M. (1986) *J. Biol. Chem. 261*, 6107−18.
6. Neece, S. H., Carles-Kinch, K., Tomso, D. J., and Kreuzer, K. N. (1996) *Mol. Microbiol. 20*, 1145−54.
7. Woodworth, D. L., and Kreuzer, K. N. (1996) *Genetics 143*, 1081−90.
8. Kreuzer, K. N., and Drake, J. W. (1994) in *Molecular Biology of Bacteriophage T4* (Karam, J. D., Ed.) pp 89−97, American Society for Microbiology, Washington DC.
9. Formosa, T., and Alberts, B. M. (1986) *Cell 47*, 793−806.
10. Hinton, D. M., and Nossal, N. G. (1986) *J. Biol. Chem. 261*, 5663−73.
11. Yonesaki, T., Ryo, Y., Minagawa, T., and Takahashi, H. (1985) *Eur. J. Biochem. 148*, 127−34.
12. Ando, R. A., and Morrical, S. W. (1998) *J. Mol. Biol. 283*, 785−96.
13. Kodadek, T., Gan, D. C., and Stemke-Hale, K. (1989) *J. Biol. Chem. 264*, 16451−7.
14. Morrical, S. W., and Alberts, B. M. (1990) *J. Biol. Chem. 265*, 15096−103.
15. Melamede, R. J., and Wallace, S. S. (1977) *J. Virol. 24*, 28−40.
16. Melamede, R. J., and Wallace, S. S. (1978) *FEBS Lett 87*, 12−6.
17. Melamede, R. J., and Wallace, S. S. (1980) *Mol. Gen. Genet. 177*, 501−9.
18. Wallace, S. S., and Melamede, R. J. (1972) *J. Virol. 10*, 1159−69.
19. Morrical, S. W., Wong, M. L., and Alberts, B. M. (1991) *J. Biol. Chem. 266*, 14031−8.
20. Yassa, D. S., Chou, K. M., and Morrical, S. W. (1997) *Biochimie 79*, 275−85.
21. Yonesaki, T., and Minagawa, T. (1989) *J. Biol. Chem. 264*, 7814−20.
22. Sweezy, M. A., and Morrical, S. W. (1997) *J. Mol. Biol. 266*, 927−38.
23. Jiang, H., Salinas, F., and Kodadek, T. (1997) *Biochem. Biophys. Res. Commun. 231*, 600−5.
24. Umezu, K., Chi, N. W., and Kolodner, R. D. (1993) *Proc. Natl. Acad. Sci. U.S.A. 90*, 3875−9.
25. Webb, B. L., Cox, M. M., and Inman, R. B. (1997) *Cell 91*, 347−56.
26. Hegde, S. P., Qin, M. H., Li, X. H., Atkinson, M. A., Clark, A. J., Rajagopalan, M., and Madiraju, M. V. (1996) *Proc. Natl. Acad. Sci. U.S.A. 93*, 14468−73.
27. Liu, Y. H., Cheng, A. J., and Wang, T. C. (1998) *J. Bacteriol. 180*, 1766−70.
28. Sung, P. (1997) *J. Biol. Chem. 272*, 28194−7.
29. Sung, P. (1997) *Genes Dev. 11*, 1111−21.
30. New, J. H., Sugiyama, T., Zaitseva, E., and Kowalczykowski, S. C. (1998) *Nature 391*, 407−10.
31. Gasior, S. L., Wong, A. K., Kora, Y., Shinohara, A., and Bishop, D. K. (1998) *Genes Dev. 12*, 2208−21.
32. Hays, S. L., Firmenich, A. A., and Berg, P. (1995) *Proc. Natl. Acad. Sci. U.S.A. 92*, 6925−9.

33. Beernink, H. T. H., and Morrical, S. W. (1999) *Trends Biochem. Sci. 24*, 385−389.
34. Formosa, T., and Alberts, B. M. (1984) *Cold Spring Harbor Symp. Quant. Biol. 49*, 363−70.
35. Hurley, J. M., Chervitz, S. A., Jarvis, T. C., Singer, B. S., and Gold, L. (1993) *J. Mol. Biol. 229*, 398−418.
36. Jiang, H., Giedroc, D., and Kodadek, T. (1993) *J. Biol. Chem. 268*, 7904−11.
37. Beernink, H. T., and Morrical, S. W. (1998) *Biochemistry 37*, 5673−81.
38. Sweezy, M. A., and Morrical, S. W. (1999) *Biochemistry 38*, 936−44.
39. Alberts, B. M., and Herrick, G. (1971) *Methods Enzymol. 22*, 198−217.
40. Sambrook, J., Fritsch, E. F., and Maniatis, T. (1989) *Molecular Cloning, A Laboratory Manual*, 2nd ed., Cold Spring Harbor Press, Plainview, NY.
41. Kutter, E., Beug, A., Sluss, R., Jensen, L., and Bradley, D. (1975) *J. Mol. Biol. 99*, 591−607.
42. Favre, D. (1992) *Biotechniques 13*, 22, 25−26.
43. Gill, S. C., and von Hippel, P. H. (1989) *Anal. Biochem. 182*, 319−326.
44. Miller, H. (1987) *Methods Enzymol. 152*, 145−170.
45. Yamamoto, K. R., Alberts, B. M., Benzinger, R., Lawhorne, L., and Treiber, G. (1970) *Virology 40*, 734−44.
46. Menetski, J. P., and Kowalczykowski, S. C. (1985) *J. Mol. Biol. 181*, 281−95.
47. Ames, B. N. (1966) *Methods Enzymol. 8*, 115−118.
48. Lefebvre, S. D., and Morrical, S. W. (1997) *J. Mol. Biol. 272*, 312−26.
49. Birdsall, B., King, R. W., Wheeler, M. R., Lewis, C. A., Jr., Goode, S. R., Dunlap, R. B., and Roberts, G. C. (1983) *Anal. Biochem. 132*, 353−61.
50. Kowalczykowski, S. C., Paul, L. S., Lonberg, N., Newport, J. W., McSwiggen, J. A., and von Hippel, P. H. (1986) *Biochemistry 25*, 1226−40.
51. Yphantis, D. A. (1964) *Biochemistry 3*, 297.
52. Johnson, M. L., Correia, J. J., Yphantis, D. A., and Halvorson, H. R. (1981) *Biophys. J. 36*, 575−88.
53. Laue, T. M., Shaf, B. S., Ridgeway, T. M., and Pelletier, S. L. (1992) *Analytical Ultracentrifugation in Biochemistry and Polymer Science*, 1st ed., Royal Society of Chemistry, Cambridge, U.K.
54. Schachman, H. K. (1957) *Methods Enzymol. 4*, 32−99.
55. Stafford, W. F. (1992) *Anal. Biochem. 203*, 295−301.
56. Stafford, W. F. (1997) *Curr. Opin. Biotechnol. 8*, 14−24.
57. Alani, E., Thresher, R., Griffith, J. D., and Kolodner, R. D. (1992) *J. Mol. Biol. 227*, 54−71.
58. Silver, M. S., and Fersht, A. R. (1982) *Biochemistry 21*, 6066−72.
59. McGhee, J. D., and von Hippel, P. H. (1974) *J. Mol. Biol. 86*, 469−89.
60. Record, M. T., Jr., deHaseth, P. L., and Lohman, T. M. (1977) *Biochemistry 16*, 4791−6.
61. von Hippel, P. H., and Schleich, T. (1969) *Acc. Chem. Res. 2*, 257−265.
62. McGhee, J. D. (1976) *Biopolymers 15*, 1345−75.

BI991917H